Seasonality of the ventilation of the tropical Atlantic thermocline in an ocean general circulation model

Alban Lazar,[1] Tomoko Inui,[3,4] Paola Malanotte-Rizzoli,[3] Antonio J. Busalacchi,[1] Liping Wang,[1] and Ragu Murtugudde[1]

Received 4 October 2000; revised 3 January 2002; accepted 11 January 2002; published 14 August 2002.

[1] This paper presents an analysis of subduction and advection within the shallow subtropical-tropical connections (STC) of the Atlantic Ocean. We carried out a kinematic study of the seasonal cycle of subduction, entrainment, and subsurface circulation in an upper Atlantic Ocean general circulation model (GCM), with a particular emphasis on the southern STC that is less studied but more important for the water supply of the equatorial upwelling. It is found that the southern STC, like the northern, has a typical water mass formation rate of 25–50 m/year, depending on the wind product used. This formation lasts 1 to 2 months in the south (longer in the northern tropics) and starts from early winter to late spring, in contrast to the common view of the end of March start. Such a large span of starting time is explained by a key control mechanism of the wind through the spatial distribution and seasonal variations of its speed. Each of these results stresses the importance of the variability as well as the uncertainties of the wind forcing for understanding the sustenance and variability of the characteristics of the tropical and equatorial thermocline. The slow currents within the thermocline branches of the STC may play a role in setting an interannual to decadal timescale for tropical or equatorial SST variability; we estimate an Atlantic STC timescale associated with the main advective pathways that at maximum reaches 5 years. *INDEX TERMS:* 1620 Global Change: Climate dynamics (3309); 3319 Meteorology and Atmospheric Dynamics: General circulation; 3307 Meteorology and Atmospheric Dynamics: Boundary layer processes; *KEYWORDS:* STC, subduction, upwelling, thermocline, mixed layer

1. Introduction

[2] Recent studies aimed at understanding the low-frequency variability of the tropical oceans have hypothesized that oceanic teleconnections between subtropics and tropics could constitute the oceanic part of slow-coupled ocean-atmosphere modes [e.g., *Gu and Philander*, 1997]. Most attention has been focused on the Pacific Ocean because of the importance of El Niño southern oscillation. However, the interannual to decadal variability of the tropical Atlantic Ocean is a strong signal [e.g., *Servain*, 1991] that provides strong motivation for studying the physics of subtropical-tropical connections within this basin. Various mechanisms could be at play within these connections involving either perturbations of the mean circulation [*Lu and McCreary*, 1995; *Liu*, 1999; *Huang and Pedlosky*, 1999; *Inui et al.*, 2002], propagation of anomalous signals within the mean circulation [*Schneider et al.* 1998; *Lazar et al.*, 2001], or both [*Schneider*, 2000]. It is reasonable to think that subduction of water masses in the tropics and low subtropics has a significant role in affecting the tropical and equatorial thermocline characteristics, and from there it is conceivable that low-frequency variability of the subduction is partly influencing interannual or decadal sea surface temperature variability.

[3] Progress substantiating any of these hypotheses will require a better knowledge of the sources and the circulation of the shallow subtropical-tropical cells (STC) that form the oceanic thermocline connections. In the low tropical Atlantic Ocean, the mixed layer flow is dominated by poleward transport except in the Southern Hemisphere within the north Brazil boundary current (NBC) [*Blanke et al.*, 1999]. Therefore the subsurface equatorward branches of the STC provide the major connections from the subtropics to the tropics. Low-frequency changes in the subduction might alter their structure, which is why we want to understand the ventilation process in the first place. Hence in this paper, we provide basin-scale information on the seasonal cycle of formation and circulation of low latitude subsurface shallow water masses.

[4] Regarding the ventilation of tropical thermocline water and the surface sources of the subsurface limb of the STC, numerous studies of the subduction in the North Atlantic have been carried out [e.g., *Marshall et al.*, 1993

[1]ESSIC, University of Maryland, College Park, Maryland, USA.
[2]Now at Laboratoire d'Océanographie Dynamique et de Climatologie (LODYC), Université Pierre et Marie Curie, Paris, France.
[3]Massachusetts Institute of Technology, Cambridge, Massachusetts, USA.
[4]Now at International Arctic Research Center, University of Alaska, Fairbanks, Alaska, USA.

0148-0227/02/2000JC000667$09.00

(hereinafter referred to as MNW93); *Williams et al.*, 1995; *Marshall et al.*, 1999]. They developed a clear picture of the rate and duration of water mass formation in the northern basin, the results of which will be recalled in detail later in the present paper. On the other hand, no basin-scale analysis of these processes has been conducted in the South Atlantic and, despite the fact that the Southern Hemisphere provides nearly all the water of the upper equatorial thermocline.

[5] After identifying the sources within the mixed layer, we proceed to characterize of the subsurface branches of the Atlantic STC by identifying the pathways and the timescale associated with the circulation. Several recent studies succeeded in providing a global description of these pathways, especially in annual mean [e.g., *Blanke et al.*, 1999; *Malanotte-Rizzoli et al.*, 2000]. However, our knowledge of their seasonal variation, at subsurface in particular, is still essentially based upon localized studies. Thus more global basin-scale approaches to the question are required. For example, the strong seasonality of surface currents, particularly in the north, is associated with strong subsurface seasonality of the currents, especially as manifested in the heat transport [*Hastenrath and Merle*, 1986]. However, the variability of the subsurface flow was investigated with a 2.5 layer model by *Lee and Csanady* [1999], who found it to be essentially limited to the equatorial undercurrent (EUC). Such results need further examination since it is reasonable to think that the high variability of the north equatorial countercurrent (NECC) has an imprint below the mixed layer. Of particular relevance to the study of interannual to decadal variability is the determination of the integrated effect of the seasonally varying circulation on the several-year journey of the water masses within the tropical thermocline.

[6] The present work uses output from an Atlantic Ocean GCM to provide a basin-scale depiction of the formation and circulation of the tropical thermocline water. We first diagnose the impact of the seasonal cycle on the rate, time and duration of the subduction using kinematic methods (section 3). We also discuss the validity of the results by comparison with some simple observational analyses. Then we diagnose the seasonal circulation within the core of the thermocline in term of conservative quantities. This enables us to discuss the timescale and the trajectories of the water masses over several years (section 4). Again we validate conclusions by intercomparison with some available observations. A concluding section summarizes and discusses the results of this work.

2. Model and Its Ocean Mixed Layer

2.1. Ocean Model

[7] We employ a reduced-gravity, primitive equation OGCM [*Gent and Cane*, 1989] coupled to an advective atmospheric mixed layer model (AML) [*Seager et al.*, 1995]. Its Pacific and Indian versions are described extensively by *Murtugudde and Busalacchi* [1998] and *Murtugudde et al.* [2000]. The Atlantic model domain used here is described by *Inui et al.* [2002]. It spans (50°N, 50°S) × (100°W, 20°E) with a horizontal resolution of 1/2°. The vertical structure of the upper ocean model consists of a mixed layer and 19 active layers below. Like temperature, salinity, horizontal currents and mixed layer depth, the thickness of the deepest active layer is computed prognostically. The remaining layers are computed diagnostically such that the ratio of each layer to the total depth below the mixed layer is held to its prescribed value (they are sigma layers, not isopycnal layers). As a result the resolution is enhanced just below the mixed layer, with typical annually averaged layer thickness in the tropics ranging from about 10 m (layers 1–4), to 20 m (5–8), to 40 m (9–11), to 60 m (12–14), to 100 m (15–16), to 200 m (17), to 300 m (18–19). The deepest active layer is bounded at the bottom by an isopycnal surface and an inactive bottom layer below, both of which with a density of 1027.8 chosen because it corresponds in the *Levitus and Boyer* [1994] data to the 4°C isotherm, considered the lower limit of the thermocline. The potential density is computed using the UNESCO formula. The bulk mixed layer model [*Kraus and Turner*, 1967] relates entrainment and detrainment to the atmospheric input of turbulent kinetic energy and buoyancy. Below the mixed layer, a gradient Richardson number closure is added to a background diffusivity of 10^{-5} m^2 s^{-1} [*Chen et al.*, 1994] to derive vertical exchange of mass and water properties between layers. Lateral mixing of water properties, layer thickness and momentum is computed along sigma layers using a high order Shapiro filter.

[8] The ocean model is forced with climatological winds [*Hellerman and Rosenstein*, 1983] and the thermohaline fluxes of the AML, which is forced with climatological precipitation [*Oberhuber*, 1988], ERBE radiation and ISCCP cloudiness. The model is spun up to a seasonal steady state with a repeated mean annual cycle of monthly varying climatological forcing fields. Our model lacks a deep circulation; its use for a diagnostic study of the Atlantic Ocean circulation must be discussed. Indeed, there may be a concern that by not resolving the lower part of the meridional overturning circulation, a reduced gravity model could underestimate the associated northward return flow of the upper ocean. This issue is partly addressed by restoring the temperature, salinity and layer thickness fields at the open ocean lateral boundaries toward the observed vertical profiles. Specifically, these quantities are relaxed to values computed from the *Levitus and Boyer* [1994] data in sponge layers over latitudes 55°–60° north and south, over longitudes 17°E–20°E south of Africa and over 9°W–11°W at the Strait of Gibraltar. Even though the velocities are set to zero at these open boundaries (no slip conditions), the sponge layer restoration allows for net mass flow in and out of the domain in each layer. These conditions create the observed net meridional pressure gradient and mass flux between the two polar boundaries that drives the upper limb of the meridional circulation. However, away from the open boundaries the distribution of this northward return flow may be altered by the reduced gravity approximation (i.e. the absence of deep flow and influences of topography). For this reason, we present several comparisons of the simulated fields with the observations, and we show that the characteristics of the model circulation discussed here are adequately realistic for the purposes of our study. In particular, for the depth interval we are interested in (the upper 500 m depth), the model simulates a net northward mass transport across the equator of 7 Sv (1 Sv = 10^6 m^3 s^{-1}). This value lies on the low side of recent OGCM simulations: the FLAME simulations [*Kröger*, 2001] reach a value of 10 Sv,

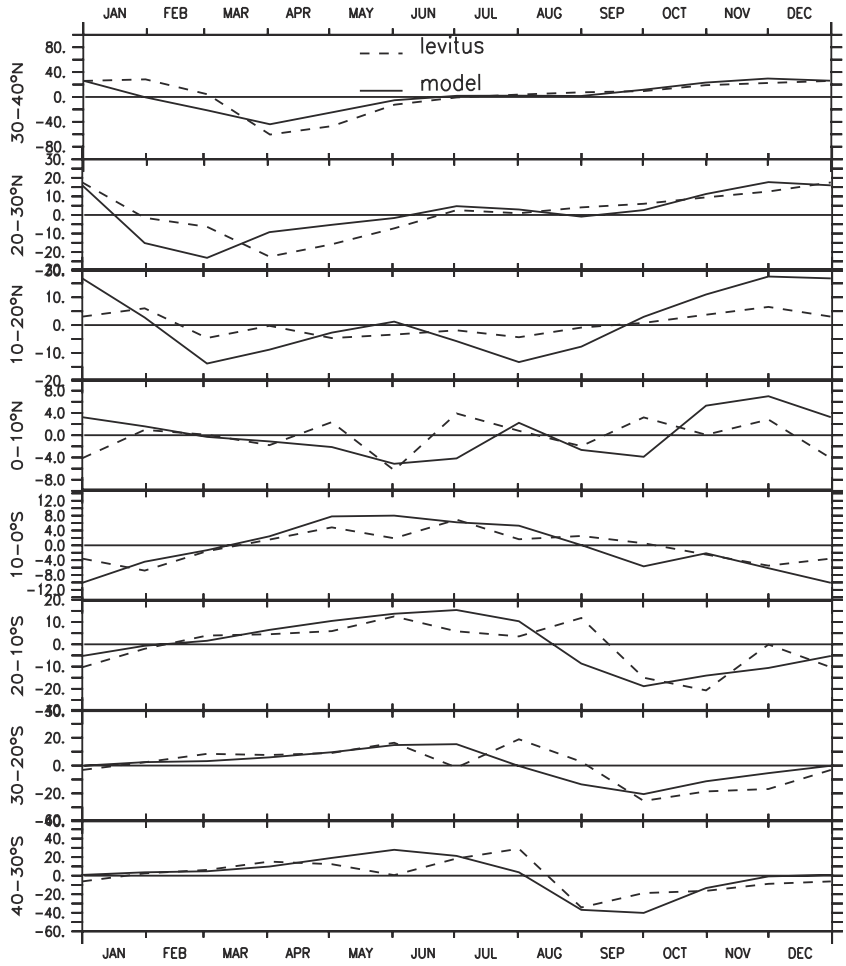

Figure 1. Time derivative of the monthly mean mixed layer depths (m/month) laterally averaged within 10° latitude bands computed from the *Levitus and Boyer* [1994] data (dashed) and the reference simulation (solid).

whereas the OPA OGCM, which is known to slightly overestimate the interhemispheric transport [*Blanke et al.*, 1999] reaches 12 Sv for the same depth interval. In our simulation such an underestimated upper ocean cross-equatorial transport does not significantly affect the quantification study of the subduction cycle (subduction rate, starting time and duration), as it is shown hereafter by favorable comparisons with the literature and the observations. Regarding the subsurface diagnostics presented in section 4, this characteristic could correspond to underestimated northward velocities within the upper thermocline south equatorial current (SEC). In fact, as discussed section 4c, these velocities have the correct order of magnitude, suggesting that this weakness of the model is confined to western boundary thermohaline currents, and that our subsurface analysis, focused on open ocean circulation mainly wind driven, is correct.

2.2. Annual Cycle of the Mixed Layer

[9] The bulk mixed layer model we used has a maximum allowable depth of 150 m. This prevents the model from correctly simulating the subduction cycle poleward of approximately 35–40° of latitude, depending on hemisphere. Consequently we will limit our discussion to the results in the subdomain 40°N–40°S. The mixed layer depths in our simulation are generally deeper by 20 m (at low latitudes) to 50 m than the mixed layers computed by *Levitus and Boyer* [1994], where the comparable calculation uses a criterion of vertical density difference with the surface of less than 0.125 kg m^3). This discrepancy is not deemed of primary importance since one of our goals here is to identify the changes in the mixed layer throughout the course of the year that affect the formation and subduction of the tropical thermocline water masses. In this case, the quantities that the model must simulate most correctly are the local amplitudes and phases of the mixed layer's seasonal variations, since these control the subduction and obduction [*Qiu and Huang*, 1995] instantaneous fluxes and their timing. A validation of the timing of the mixed layer depth variations follows, but before that, we check the amplitude of these variations. This is given by the time derivative of the monthly mean mixed layer depth, which is plotted for the Levitus and Boyer data and our simulation Figure 1, for zonal averages in 10° latitude bands. It appears that the bulk mixed layer model reproduces reasonably the amplitude of the changes at midlatitude with a phase shift of at most one month, which is an acceptable difference for a monthly mean value comparison. Equatorward of 20° of

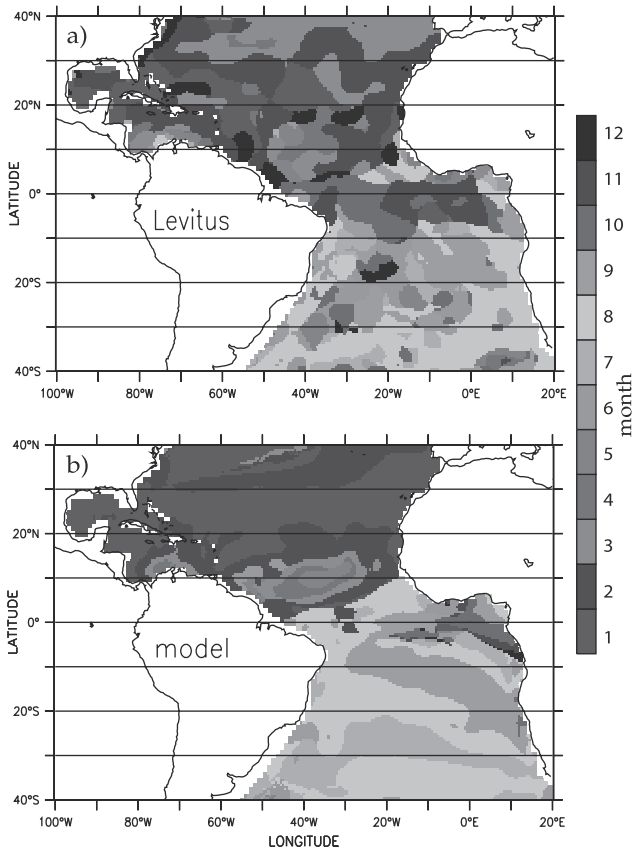

Figure 2. Horizontal distribution of the month (from 1 to 12 for January to December) of deepest mixed layer. (a) *Levitus and Boyer* [1994] data set. (b) Reference simulation. See color version of this figure at back of this issue.

latitude, the overall comparison is a bit less favorable with less clear cycles, but the simulation of the main shallowing event (negative values) at the end of the winter season is satisfying. It occurs at the same time in the model as in the observations in the 0–10°N and 10–20°N bands (February–March), and with only a 1-month difference in the corresponding Southern Hemisphere's bands (the model is earlier: in Sept.–Oct. within 0–10°N, and Aug.–Sept. within 10–20°N).

[10] For the validation of the timing of the mixed layer cycle, which sets the season of water mass formation, we neglect the divergence of the mixed layer currents and consider any mixed layer shallowing event as a potential subduction event. This way, direct comparison with the *Levitus and Boyer* [1994] mixed layer cycle is possible. In the next section we will consider the full simulated subduction-obduction that includes the divergence of mixed layer currents. Figure 2 displays the horizontal distribution of the time of deepest mixed layer for the model and climatology. In subsequent times the mixed layer shoals presumably marking the beginning of the subduction period. This represents the simplest estimate of the starting months of subduction one can obtain from raw mixed layer depth observations. In the simulation (Figure 2b), the shallowing in the Northern Hemisphere starts in January across a large subtropical band within the basin, and subsequently spreads around this band in February–March. In Spring the process moves to the 10–20° latitude band until May. In the Southern Hemisphere, we find a somewhat comparable cycle with a starting period in July within a band somewhat symmetric about the equator to the Northern Hemisphere January band, then in August it expands meridionally (up to the equator along Brazil). Then in September the mixed layer reaches its maximum depth in a large band spreading from the Eastern subtropics to the western tropics and eventually the cycle ends in the equatorial band (with large January–February patches). The comparison with the field computed from the Levitus and Boyer data (Figure 2a) is largely favorable in the Northern Hemisphere except for the January band that does not reach the eastern basin in this data set. The similarity is less striking in the south: north of 30°S, we find a similar starting patch in the center of the basin (spreading more to the north), but one to two months earlier, then the surroundings are reached in August with a late September patch in the east tropics, comparable but smaller to the simulation. Again the cycle terminates at the equator in January.

[11] The discrepancy in the south may be largely due to the uncertainties in the observations for this basin (wind forcing as well as mixed layer depth). For example, the same model forced by the *Da Silva et al.* [1994] wind product generates a central July pattern larger toward the equator and a reduced September patch (not shown). However, it is clear that the run forced by the *Hellerman and Rosenstein* [1983] winds simulates the late northern tropical pattern of deep mixed layer much better than does the Da Silva et al. run.

3. Subduction Cycle

3.1. Annual Subduction Rate

[12] Following *Cushman-Roisin* [1987], the instantaneous subduction rate is the volume flux of mixed layer fluid entering the thermocline per unit horizontal area; neglecting evaporation and precipitation, it is defined by

$$S(t) = -\partial h/\partial t - (\partial(hu)/\partial x + \partial(hv)/\partial y). \qquad (1)$$

The first right hand term is the change of mixed layer depth h and the second is the lateral divergence of the assumed vertically homogeneous mixed layer currents. Hence the instantaneous subduction rate at the base of the mixed layer in our model is simply obtained by subtracting the mixed layer depth time derivative from the convergence of the mixed layer transport $h\mathbf{u}$ (with $\mathbf{u}$ the horizontal velocity vector of the bulk mixed layer).

[13] In order to determine where the water masses of the subtropical and tropical upper Atlantic are formed and at what rate, we need to calculate the annual subduction rate S_{ann} over the basin. This quantity differs greatly from the annual average of the instantaneous subduction rate since outside of the effective subduction period (end of winter and spring as discussed next chapter) fluid temporarily subducts into the seasonal thermocline but is then re-entrained into the mixed layer during winter [*Cushman-Roisin*, 1987]. Using the kinematic formulation proposed by *Marshall and Marshall* [1995] and *Marshall et al.* [1999] we identify S_{ann} with the annual volume flux across the Eulerian interface $z = -H(x, y)$ representing the base of the deepest mixed

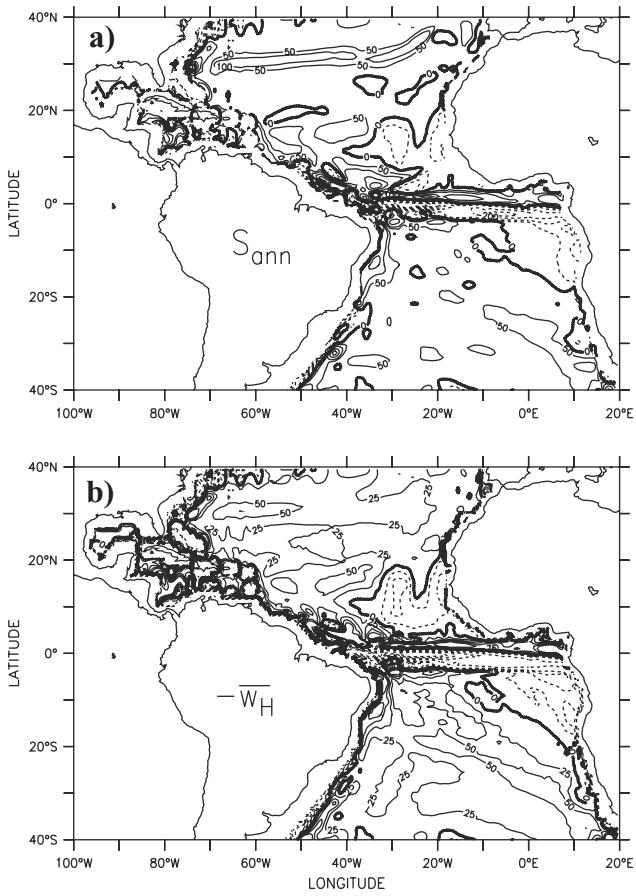

Figure 3. Kinematic calculation for (a) annual subduction rate S_{ann} into the main thermocline, c.i. = 50 m/year, (b) annual vertical flux into the main thermocline, c.i. = 25 m/year. Negative values indicate entrainment into the seasonal thermocline or the mixed layer.

layer at a given location (a definition of the top of the permanent thermocline):

$$S_{ann} = -\left(\overline{V_H} \cdot \nabla H + \overline{w_H}\right) \quad (2)$$

with $\overline{V_H}$ and $\overline{w_H}$ the annual mean horizontal and vertical velocity at the depth H. The model-derived annual subduction rate is shown Figure 3a. The large-scale pattern is characterized by four main regimes in the Northern Hemisphere. At the southern edge of the Gulf Stream and northern branch of the subtropical gyre, S_{ann} is strongly positive (up to 200 m/year) due to the equatorward advection of water by the gyre below the (equatorward) shoaling mixed layer [*Williams et al.*, 1995]. In the subtropical region and the western tropics, S_{ann} is around 50 m/year mainly as a result of surface current convergences and associated downwellings (Figure 3b). The eastern tropics are characterized by entrainment due essentially to negative Ekman pumping. Note the strong positive pattern in the west around 5°N where the NECC flows eastward into the shoaling permanent thermocline. Except north of the midlatitude front where S_{ann} is incorrect (it should be an intense entrainment area) due to the artificial limit to mixed layer depths in our model, these broad patterns are in good agreement with those found by *Williams et al.* [1995] and *Marshall et al.* [1999] in their North Atlantic model studies. When compared to the recent Lagrangian calculation by *Blanke et al.* [2002], the rates have comparable order of magnitude, but there is a few degree downstream shift of the northern and southern salinity maximum waters (respectively centered at 20°N and 15°S) that reflects a systematic error associated with Eulerian calculation within the north equatorial current and the SEC.

[14] Assessment of the Southern Hemisphere subduction rate is an important result of our study since no large-scale depiction of it exists in the literature, and this basin plays a key role in the tropical Atlantic climate. Indeed the Southern Hemisphere provides most of the water making up the upper thermocline of the tropical Atlantic [*Wilson et al.*, 1994; *Stramma and England*, 1999]. Figure 3 shows that Southern Hemisphere S_{ann} has a much more regular distribution than in the north, and apart from the upwelling region in the eastern tropics, it is characterized by subduction at a rate of about 50 m/year. As in the north, the tropical entrainment region corresponds principally to the divergent Ekman transport associated with the trade winds. In contrast with the north, interior currents south of the equator do not impose a very important structure on the S_{ann} field, nor are they large mixed-layer fronts as at the southern edge of the Gulf Stream. Consequently, S_{ann} is in large part related to moderate downward pumping. Note though that due to the 150 m mixed layer depth limit, the ocean model is unable to correctly simulate the large production rate of south Atlantic mode water which occurs south of approximately 35°S [see, e.g., *De Miranda et al.*, 1999].

[15] As suggested by these results, wind forcing is the dominant factor determining the annual subduction rate, especially in the eastern tropics and parts of the Southern Hemisphere. In view of this dependency, we also computed S_{ann} for a simulation forced by the *Da Silva et al.* [1994] wind product, which is characterized by generally weaker stresses than *Hellerman and Rosenstein* [1983] climatology [*Inui et al.*, 2002]. This experiment had weaker subduction and obduction rates by a factor close to 2, principally in the tropics (not shown). This result emphasizes the requirement for an accurate wind climatology to correctly monitor the variability in the mass and temperature-salinity sources of the tropical thermocline.

3.2. Starting Time of Subduction

[16] Having determined the annual subduction rate, we next identify the month at which the shallowing mixed layer first starts to isolate water from atmospheric fluxes. Given the instantaneous subduction rate from equation (1), we computed in our simulation the time W_1 of the first subduction event, $S(W_1)>0$, that occurs after the time of maximum local mixed layer depth. This criterion was chosen because as noted earlier, any waters subducted before the mixed layer reaches its maximum depth have no time to leave the area and are re-entrained into the mixed layer and have their properties reset to new characteristics. Our definition is directly linked to instantaneous subduction and is consequently less indirect than those used by MNW93 or *Williams et al.* [1995]. The first of these studies, which made the approximation that W_1 corresponds to the change of sign of the buoyancy flux into the mixed layer,

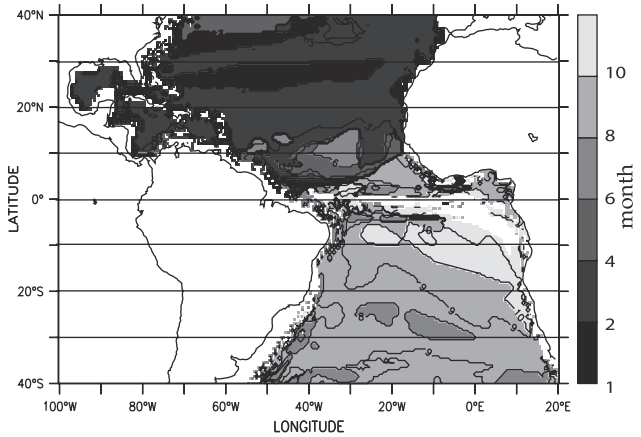

Figure 4. First month (from 1 to 12 for January to December) corresponding to net subduction into the thermocline computed from monthly mean of instantaneous subduction rate $S(t)$.

neglected the role of wind stirring (that can support entrainment at the base of the mixed layer) in the cycle of subduction. The second study, which took W_1 as the time of local density maximum (change of sign of the total buoyancy flux), neglected the possibility of having a density maximum at the same time as a deepening of the mixed layer due to an increase of the wind stirring.

[17] Figure 4 displays the horizontal distribution of W_1. The pattern is similar in the north to Figure 2 with a central region of first subduction in January, spreading to the rest of the subtropics, and continuing in the tropical area up to July. Subduction occurs from January to March in the Gulf Stream area, but we will not discuss this area in any detail since the water is entrained farther east later where the mixed layer is deeper (not net subduction, MNW93). In the south, the W_1 cycle is still characterized by a July central starting region (near 25°S), spreading in August to the rest of the subtropics, then in September to the midlatitudes and the tropics, and eventually in October in the eastern tropics. It is apparent that subduction in the subtropical and tropical Atlantic does not start everywhere at the end of winter as it is commonly thought. If one looks specifically at the regions of positive subduction (see Figure 3), the range of starting time spans a four month interval in the south and five in the north.

[18] Understanding what processes are responsible for such a spread in the starting time of subduction is important in the context of low-frequency STC variability. The two main driving forces of the mixed layer seasonal cycle are the seasonal cycles of the net short wave radiation penetrating into the ocean, and of the wind speed controlling both the entrainment at the base of the mixed layer and the latent heat loss at the surface. In order to distinguish the role of these two forcing terms in producing the spatial patterns of W_1, we performed two additional simulations. In the first, the model was spun up to a steady seasonal cycle after having filtered out any seasonality in the incoming short wave radiation (using its annual mean). In the second, it is the seasonality of the wind speed that was filtered out of the forcing of the mixed layer and AML models to obtain the steady seasonal cycle. The two corresponding maps of W_1 reveal striking differences (Figure 5) when compared to the reference simulation. For the run with steady wind speed (Figure 5a), the subduction cycle is well reproduced in the north only within a diagonal band, roughly subtropical, extending from 15°N to 30°N in the west and from 18°N to 40°N in the east. In the south, the W_1 patterns are correctly simulated at subtropical and mid latitudes. In contrast, for the run with steady short wave radiation (Figure 5b), W_1 is comparable to our control run (Figure 4) in the regions incorrectly simulated by the steady wind run, but wrong elsewhere. This implies that the seasonal cycle in the short wave radiation plays a major role in determining the timing of the subduction within the subtropics, whereas it is the cycle of the winds that controls the timing of the subduction in the tropics and also at midlatitudes in the north. We are currently investigating the details of these results and the conclusions will be presented in a subsequent paper. In the meantime, preliminary analyses of the mixed layer scheme indicate that in regions of relatively weak winds like the subtropics (corresponding to the subsidence of the Hadley cell), shallowing of the mixed layer (and associated subduction) starts when the short wave radiation flux begins to increase in January in the north and July in the south. In the tropics and midlatitudes though, especially in the north, the trade and westerly winds are associated with much stronger wind speeds and consequently stronger wind stirring and latent heat loss. Therefore, the shallowing of the mixed

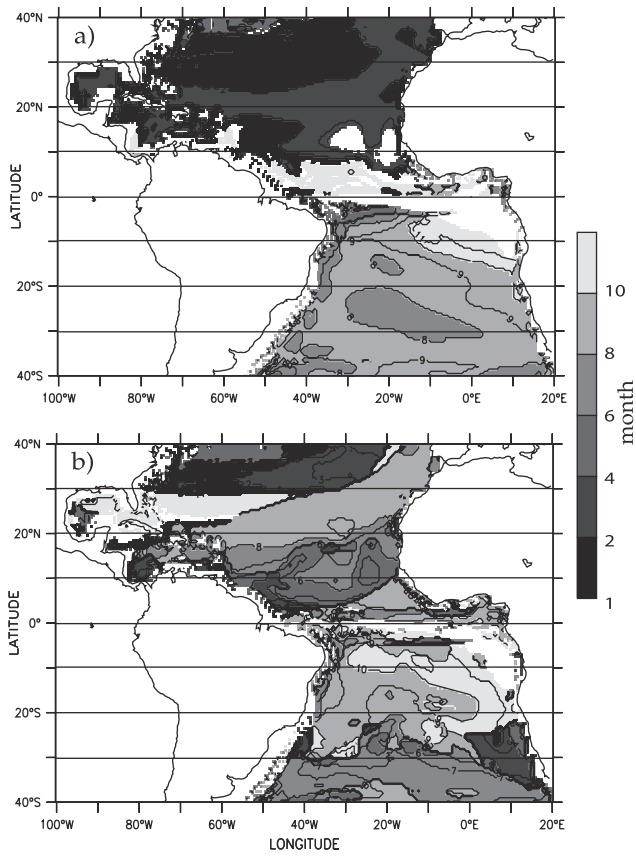

Figure 5. Same as Figure 4 but for a simulation (a) where the wind speed is kept constant to its annual mean value and (b) where the incoming short wave flux is kept constant to its annual mean value.

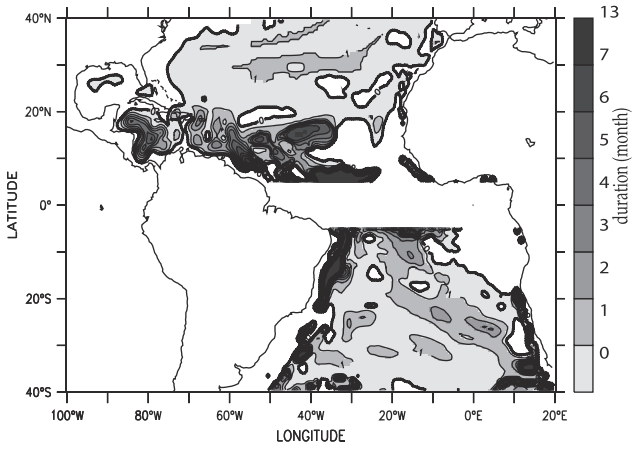

Figure 6. Subduction duration in months inferred from the kinematic estimate of the annual subduction rate, the starting time of subduction and the instantaneous subduction rate, c.i. = 1 month (up to 7). The duration is not computed in entrainment regions (see section 3.3) and in the 5N−5S latitude band.

layer begins later in the year when these winds diminish enough to allow the stratification of the mixed layer, or when the shortwave radiation increases enough to overcome the effect (mixing and latent heat loss) of the wind speed. This is why the seasonal cycle of the wind is so important in setting W_1 in the tropics and midlatitudes as illustrated by these two sensitivity experiments.

3.3. Subduction Period

[19] The subduction period τ_{eff} provides fundamental information about the properties of the subducted water masses; it is the time over which the amount of water S_{ann} is irreversibly isolated from the mixed layer by the shallowing mixed layer. The shorter this period, the more the thermocline water properties will be biased toward winter characteristics, and conversely. Following MNW93 we diagnosed τ_{eff} from the temporal evolution of $S(t)$ and the knowledge of S_{ann}, and W_1, using the following equality:

$$S_{ann} = \frac{1}{\tau_{year}} \int_{W_1}^{W_1+\tau_{eff}} S(t)dt \qquad (3)$$

Whereas a period can also be computed for negative subduction (entrainment) regions, we chose to calculate only the period of positive subduction. Indeed, as developed in the discussion chapter, the regions of entrainment are generally associated with upwelling and mixing that are thought to invalidate the kinematic calculation of the annual subduction rate there [*Marshall et al.*, 1999]. Hence Figure 6 displays S_{ann} only for the regions of positive annual rate of subduction shown in Figure 3. Note that we did not compute τ_{eff} north of the subduction front related to lateral advection by the subtropical northern gyre, since the true annual subduction is negative there even though the model has positive values for wrong reasons (see § 3a). We also masked the 5N−5S equatorial band since the field is very noisy and requires a specific study addressing the subduction−entrainment there. In the figure, one sees that the subduction period is of order one month in the subtropics and lengthens up to five or six months in the western tropics, in agreement with the previous studies of the North Atlantic. In the northern tropics the time variations of mixed layer depth are smoother and smaller than at subtropical latitudes for comparable annual subduction rate, hence several months of a shallowing mixed layer are needed to produce the appropriate amount of water. In the south, the τ_{eff} estimates are also of order one month in the subtropics, but unlike in the north, the period lengthens only weakly in the tropics (one to two months). This discrepancy is explained by a smaller annual subduction rate in the area related to less surface current divergence. In summary, our analysis confirms that the northern and southern subtropics of the Atlantic Ocean have similar short subduction periods, but shows that the tropics differ about the equator with a three to five month subduction period for the north and one to two month for the south.

4. Circulation in the Thermocline

[20] While section 3 was aimed at quantifying the influence of the seasonal cycle on the formation of the tropical thermocline water masses, in section 4 we analyze the influence of the seasonal cycle on the long-term circulation of these water masses after their subduction. We choose to detail the isopycnal σ = 25 kg m^{-3} since its circulation embodies the various types of pathways found at different levels of the subtropical-tropical circulation in the model. In order to first provide a general description of this circulation, the characteristics of its annual averaged are presented in the following paragraph.

4.1. Circulation in Annual Mean

[21] To obtain a global view of the annual mean circulation, we assume that away from the surface, the upwelling regions and the boundaries, turbulent mixing is sufficiently weak that water parcels conserve to a good approximation their density and Bernoulli function [*Rothstein et al.*, 1998] (hereinafter referred to as B) defined as:

$$B(\sigma) = \frac{1}{2}\rho_0(u^2+v^2) + \rho_0 g\ \eta + g\int_{z(\sigma)}^{0} [\rho - \rho(\sigma)]dz$$

where ρ, u and v are the density and the horizontal components of the velocity, $\sigma = \rho - 1000$ (kg m^{-3}) is associated to the isopycnal of interest and η the sea surface elevation. Based on this assumption, the flow is accurately depicted by the isopycnal projection of horizontal velocity vectors and B isolines. Alternatively, this diagnostic may be used to determine the regions where the flow becomes diabatic: the more the current vectors cross B isolines, the more the circulation has experienced mixing.

[22] Figure 7 displays the Bernoulli function and the currents on the isopycnal σ = 25 kg m^{-3}, calculated from an annual average of the seasonal circulation. Poleward of the outcrop line, the mixed layer currents are plotted. It appears that for most of the basin, the current vectors and the isolines are parallel, suggesting a largely adiabatic flow character. As expected, the regions where the isolines cross

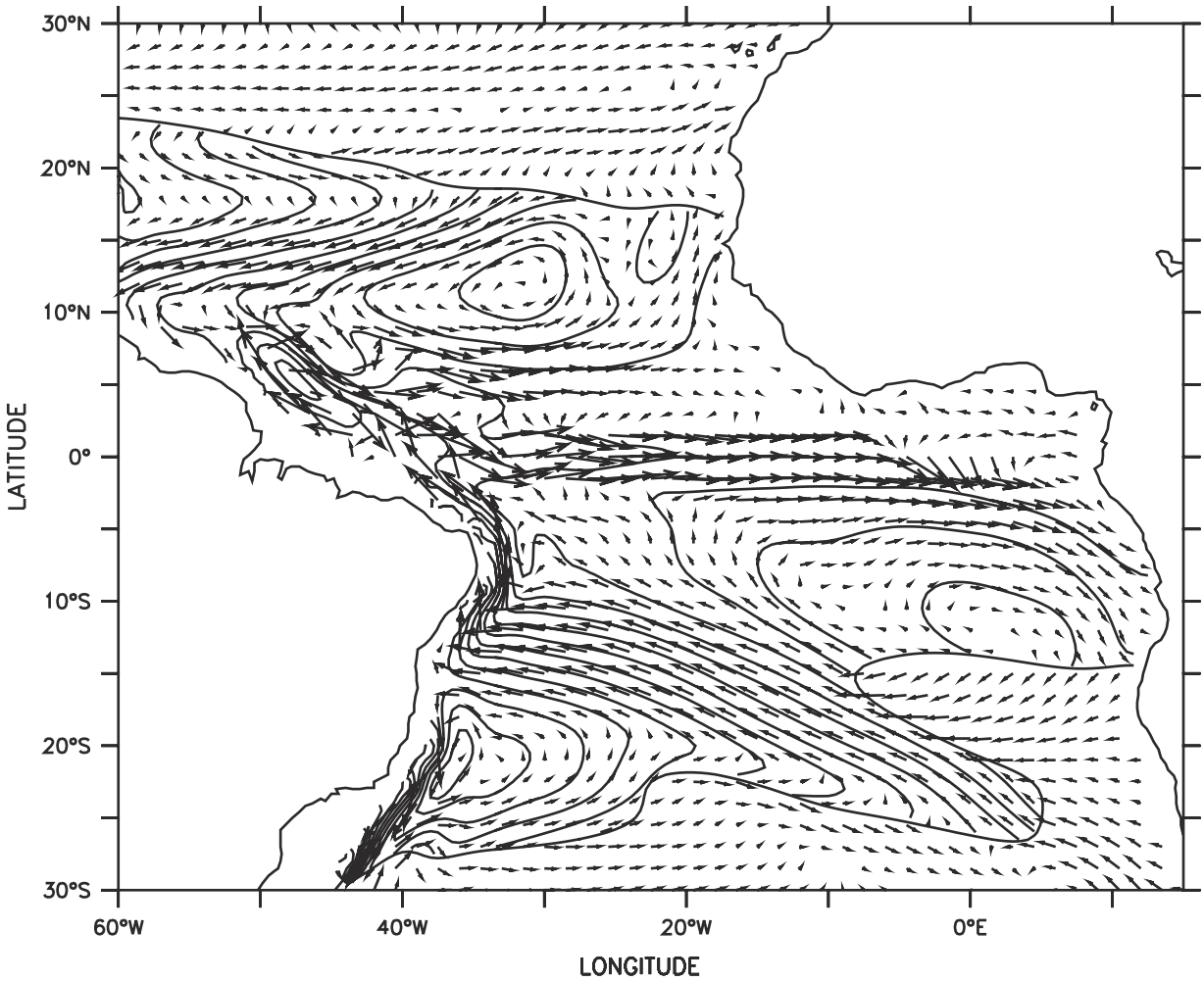

Figure 7. Bernoulli B function and horizontal current vectors for the annual mean circulation of the reference simulation. These fields are plotted along the isopycnal $\sigma = 25$ equatorward of the outcrop line (where the Bernoulli function is shown) and in the mixed layer poleward of the outcrop line (no Bernoulli function shown). The contour interval for B is 0.1 $kgs^{-2}m^{-1}$.

(and thus the flow is more diabatic) are in the 5°N–5°S equatorial band, within a few degrees of the coasts and below the regions of maximum mixed layer entrainment identified Figure 3a.

[23] The thermocline water circulation patterns simulated by the model are in good agreement with observations [i.e., *Stramma and Schott*, 1999]. Starting from the central northern position of the mean outcrop line, the north equatorial current (NEC) flows south-westward north of 10°N. Part of this flow continues equatorward off the South American coast as the Guyana undercurrent (GUC) to feed the equatorial undercurrent (EUC), either through the retroflection of the north Brazil undercurrent (NBUC) or directly through the interior. This is one of two flow pathways that connect the northern subtropics and tropics. The second pathway, adjacent to the previous one, also begins with the NEC but feeds the north equatorial undercurrent (NEUC). Although they ventilate the tropical latitudes, these waters do not reach the equator. Rather, they move northeastward to eventually either recirculate in the NEC or reach the outcrop line. This exit window is located next to Africa, east of a small gyre centered at (15°N, 20°W): the Guinea Dome (shifting northward with depth). Note that a thin westward flow at about 5°N is visible along the EUC in the central basin and the Gulf of Guinea; it corresponds to the northern branch of the south equatorial current (nSEC).

[24] In the Southern Hemisphere, the southern branch of the SEC (sSEC) occupies the central tropical basin. At the Brazilian coast the flow at the $\sigma = 25$ level bifurcates into the northward directed NBUC and southward Brazil current (BC). A second interior pathway is much broader than in the north; it is formed in the west by the equatorial branch of the SEC (eSEC). In the eastern half of the basin, the sSEC turns eastward to supply the south equatorial countercurrent (SECC) and the south equatorial undercurrent (SEUC) which together with the coastal Gabon-Congo undercurrent (GCUC) form the Angola gyre. The principal deviation from observations comes from the absence in the model of a central branch of SEC that should lie between the SECC and the SEUC. We attribute this to a lack of resolution.

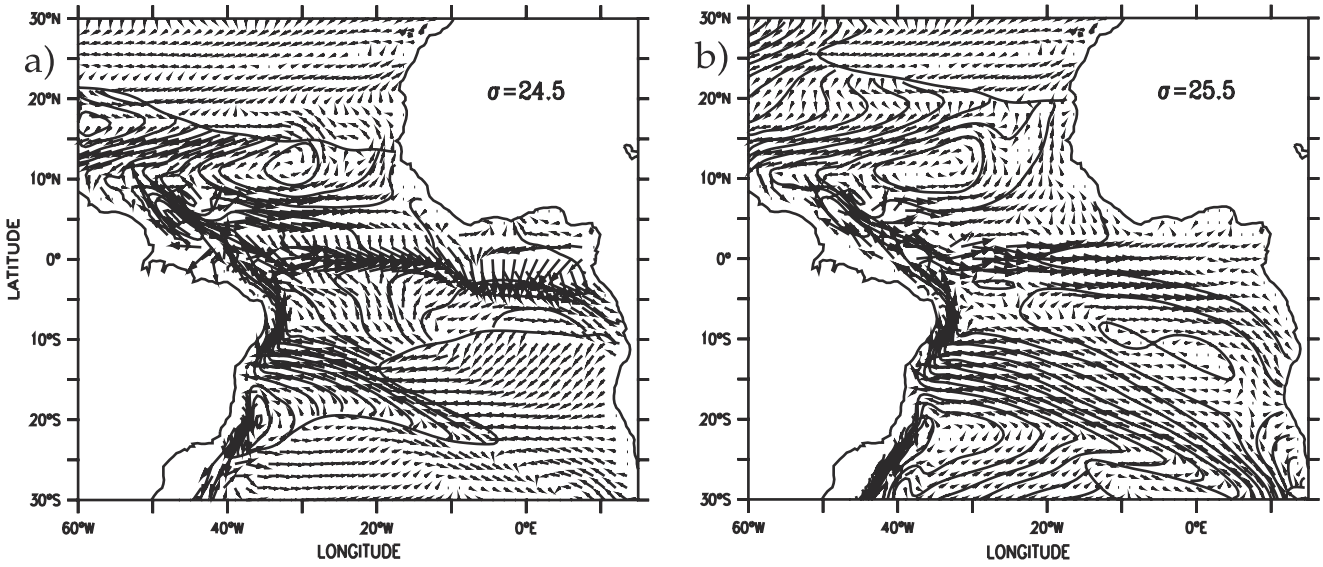

Figure 8. Same as Figure 7 but for (a) the isopycnal σ = 24.5 and (b) σ = 25.5.

[25] In order to demonstrate how well our reference isopycnal surface illustrate the thermocline pathways, we additionally present on Figure 8 the circulation and the Bernoulli function on isopycnals 24.5 and 25.5 kg m^{-3}. The main pattern is that the proportion of waters that flow equatorward through the interior versus the western boundaries diminishes with depth in both hemispheres. These patterns are in good agreement with the kinematic study of *Malanotte-Rizzoli et al.* [2000]. The sensitivity of these results to the wind product is examined by *Inui et al.* [2002], who demonstrate that the main change is in the Northern Hemisphere where the interior pathway broadens in response to *Da Silva et al.* [1994] wind product.

[26] We now look at the depth of the isopycnal as well as Q, the potential vorticity. For motion scales much larger than the Rossby deformation radius (∼50–100 km), the relative vorticity is negligible compared to the stretching term so that Q can be approximated as:

$$Q = \frac{f}{\rho_0}\frac{\partial \rho_i}{\partial z}.$$

Here f is the Coriolis parameter, and ρ_i, the in situ density. In Figure 9 one sees that the 25.5 kg m^{-3} isopycnal is shallow in the east (depths of about 25 m), with minima east of the Guinea and Angola Domes where upwelling is maximum (Figure 3b). The isopycnal deepens smoothly toward the west where it reaches maxima of about 180 m along the coast, in the regions of sSEC convergence at the coast in the south, and of the NBUC and the NEUC in the north (two regions of

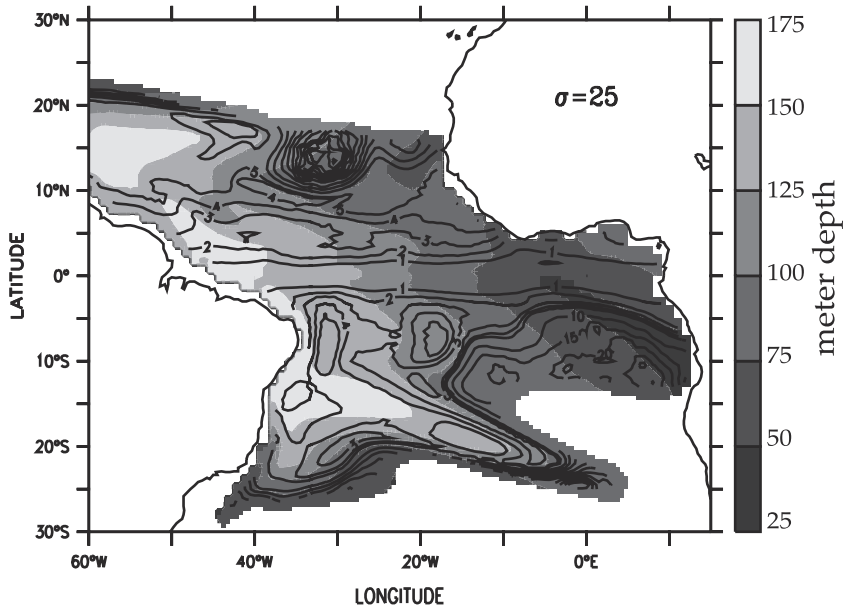

Figure 9. Isopycnal σ = 25: depth in gray (c.i. = 25 m) and potential vorticity isolines (c.i. = 10^{-10} $m^{-1}.s^{-1}$ from 0 to 5×10^{-10} $m^{-1}.s^{-1}$, and c.i.= 5×10^{-10} $m^{-1}.s^{-1}$ for higher values).

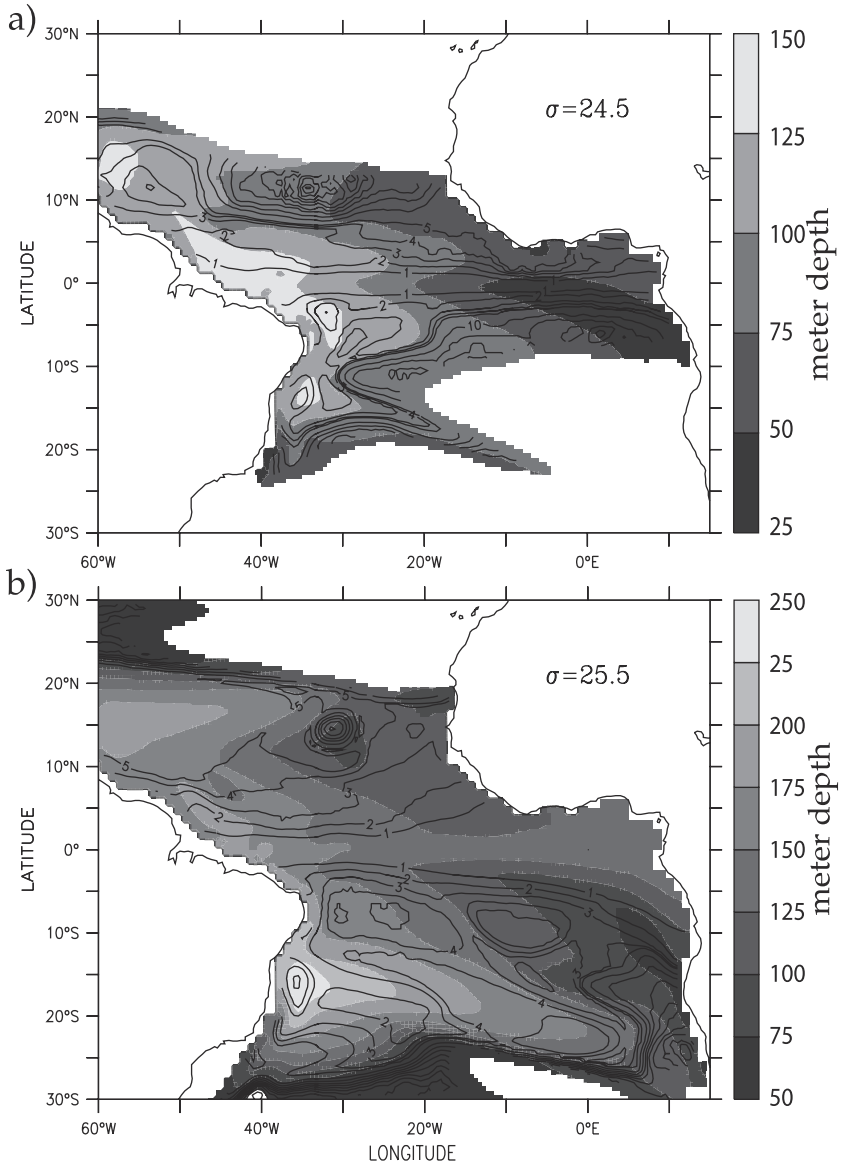

Figure 10. Same as Figure 9 but for (a) the isopycnal σ = 24.5 and (b) σ = 25.5.

strong downwelling). The potential vorticity field illustrates most of the patterns characterizing the Bernoulli function. The Absence of an elongated tongue of high potential vorticity, seen in the North Pacific [e.g., *Lu and McCreary*, 1995; *Rothstein et al.*, 1998] is particularly notable. This implies that this density class of waters in the Atlantic is able to flow toward the low tropical latitudes without passing by the western boundary (as it is visible in the Bernoulli function, Figure 7). The same fields are presented for comparison in Figure 10 for isopycnals 24.5 and 25.5. It is apparent especially in the north that the isolines within the 0°−10°N latitude band become more tilted northeastward in the east, corresponding to the closure of the interior communication pathway with depth.

4.2. Comparison with Observations

[27] In order to compare the simulated annual mean circulation with the observations, we again took the *Levitus and Boyer* [1994] data set as a reference. Due to the positive mixed layer depth bias in our model discussed earlier, the model water column is generally shifted by this same bias, which is about 50 m. Therefore in the following comparisons, we consider that the model results presented for the σ25 isopycnal correspond to the σ25.5 isopycnal in the Levitus and Boyer data set. Therefore the surface σ = 25.5 in the Levitus and Boyer data was retained as the isopycnal of comparison. As a first order estimate for the geostrophic circulation, we defined the Bernoulli function as:

$$B(\sigma) = g \int_{z(\sigma_0)}^{z(\sigma)} \rho dz$$

where σ_0 = 27.5 is the reference layer (a deeper layer makes no noticeable difference) and ρ the potential density. Comparison of the simulated and computed large-scale circulation on the two isopycnals in the Northern Hemisphere (Figure 7 and Figure 11a) indicates that the main

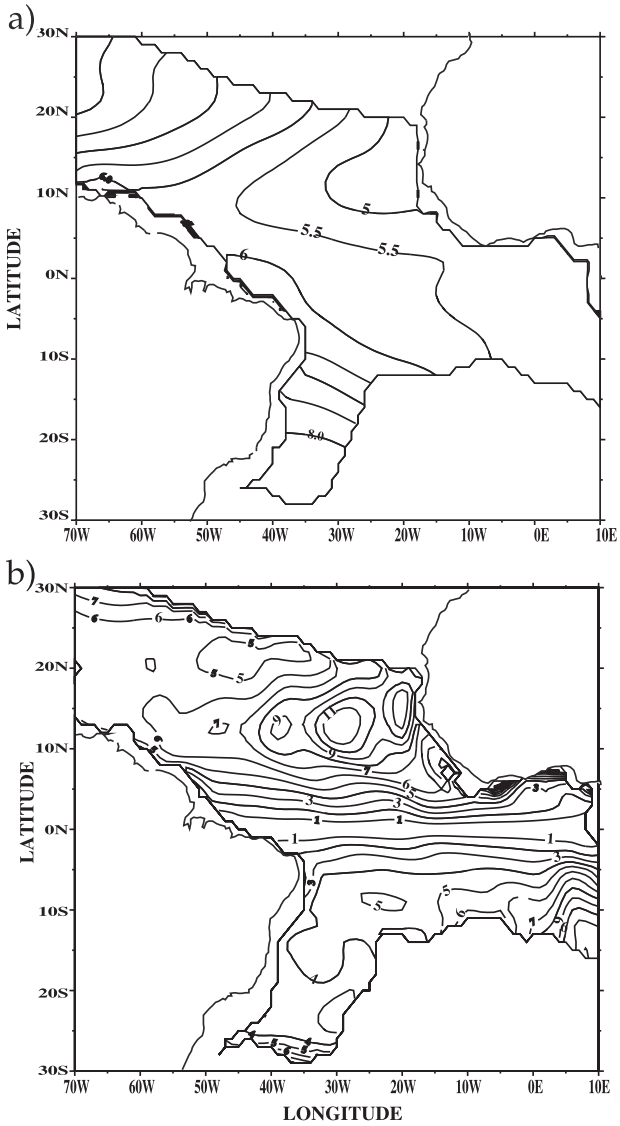

Figure 11. Conservative quantities associated with the geostrophic circulation on isopycnal σ = 25.5 in annual mean computed from *Levitus and Boyer* [1994] data. (a) Bernoulli function (c.i. = 0.5 $kg.s^{-2}.m^{-1}$). (b) Potential vorticity (c.i. = 10^{-10} $m^{-1}.s^{-1}$); the absolute value is plotted in the Southern Hemisphere.

features of the observed large-scale circulation, for example, the NEUC (in the latitude band near 6°N and centered around 30°W) and the NEC, are well simulated by the model. Furthermore, as in the model (Figure 7), the subducted water mass splits into the three branches as it moves southward. The western branch moves southwestward to reach the western boundary and eventually recirculates back to the midlatitude North Atlantic. The eastern branch moves southwestward and then eastward to reach the eastern boundary. Between these branches, the water mass moves equatorward to eventually join the equatorial undercurrent. Corresponding to this similarity in the circulation structures, the potential vorticity structures are also comparable (Figure 10 and Figure 11b).

[28] Comparison in the south is more problematic. The latitudinal extension of the isopycnal surface is larger in the simulation, and the Bernoulli function as well as the Lagrangian trajectories computed from observations shows no indication of the Angola gyre. On the other hand, this gyre appears on the potential vorticity field as a maximum. The large uncertainties in the Levitus and Boyer data set in the southeastern tropics are likely the cause of these discrepancies. Hence we think that the simulated southeastern trajectories are more realistic than those computed from observations. The comparison of these various quantities for other isopycnal surfaces gives similar general results regarding the overall large-scale circulation, the trajectories and the timescales (not shown).

4.3. Seasonal Cycle of the Circulation Along σ = 25

[29] Knowing the annual mean circulation, we next study the amplitude of its seasonal variations. Figure 12 displays the circulation for March and September for the same σ = 25 isopycnal, as well as the difference. We superimposed the corresponding Bernoulli function; for the difference plot, the smallness of the nonlinear term in B allowed us to display simply the absolute value of the difference of the two seasonal Bernoulli functions and obtain a very good stream function to visualize the circulation difference. It is important to recall that B is a conservative quantity in a stationary adiabatic circulation. In other words, the validity of the formulation of B that we are using here is limited precisely to flows with negligible time derivative. Therefore, in addition to the limitation related to the diabatic character of the flow, flow crossing B isolines indicates that circulation is varying too rapidly for the steady state formulation of B to be valid. Satisfyingly, we note that most of the flow follows the B isolines and conclude that this diagnostic is helpful in describing the circulation patterns, even for our nonsteady flow.

[30] Deviations of currents from the time mean (compare with Figure 7) are clearly apparent in both location as well as intensity. As expected, strong variability in the intensity and eastern extension of the NEUC as well as that of the NEC mark the Northern Hemisphere. In winter, the more equatorial location of the ITCZ weakens the whole northern circulation and particularly the NEUC, favoring interior connections between the outcrop line and the equator. In contrast, the northward migration of the ITCZ in summer forces much more zonal and intense flows, and all the water coming from the outcrop line flows in the NEC first to the western boundary before some eventually reaches the equator. In the south, a narrow sSEC, a weak interior flow, and a very southern location of the outcrop line characterize the end of the boreal winter, whereas a broader sSEC and stronger currents mark the boreal summer. Globally, the variability of this circulation is characterized by important variations of the pathways in the Northern Hemisphere in relation with the seasonal migration of the ITCZ (Figure 12c). Comparatively in the south, the pathways are much less variable but the associated isopycnal outcrop lines experience a large seasonal span of their positions.

4.4. Particle Trajectories Along σ = 25

[31] In view of the considerable variability in the seasonal circulation, two main questions come to mind. What is the

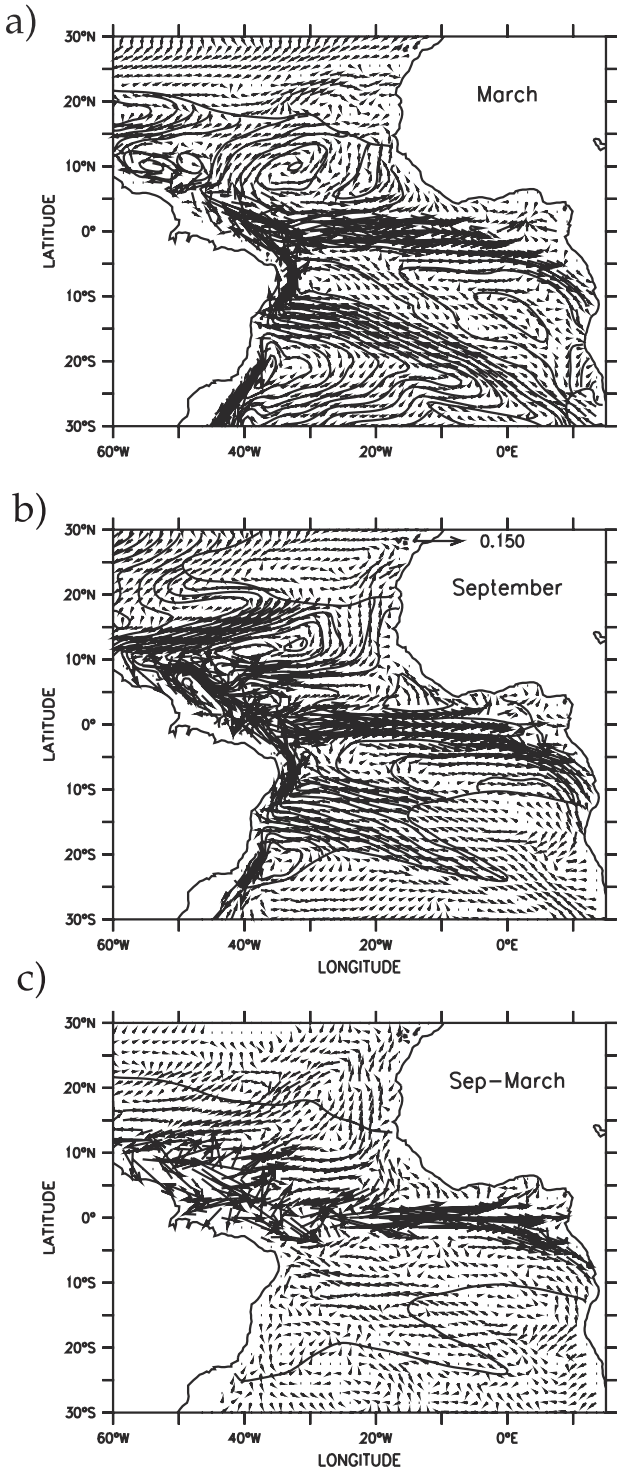

Figure 12. Same as Figure 7 but for the monthly mean circulation of (a) March and (b) September. (c) Current vectors for the September minus March circulation (overlaid over the portion of the surface common to the two months).

integrated circulation pattern of the water masses resulting from their journey within this circulation? And, what are the resulting timescales of the integrated trajectories? In order to answer these questions, we injected floats at the outcrop line of the $\sigma = 25$ isopycnal of the seasonally varying circulation and followed their trajectories over five years. The procedure we adopted was the same as by *Lazar et al.* [2001] and *Rothstein et al.* [1998] where the floats are released below the mixed layer and advected by the monthly mean horizontal currents projected along isopycnals. This calculation has the advantage of its greater simplicity compared to a calculation using rather the full three dimensional velocity field, but its validity is consequently limited to regions of low diapycnal velocities and small-scale mixing. Hence when looking at the float trajectories, one should trust more the results in the interior ocean away from the boundaries and the strong upwelling regions identified in Figure 3b (central equator and eastern tropics). Note that when a particle is re-entrained into the mixed layer, the advection computation is done with mixed layer currents. The initial location of the trajectories was chosen to span the region where water flows inside the tropical thermocline (no floats were injected in the equatorward branch of the subtropical gyre).

[32] Figure 13 shows the trajectories of floats released along the outcrop line in the north in March (hence the outcrop lines corresponds to those in Figure 12a). Departing from near 15°N, one group of particles moves toward the western boundary in the NEC and reaches the equator through the NBC retroflection in less than three years, and possibly reaches the Gulf of Guinea in approximately four years (assuming vertical mixing does not cause them leave the isopycnal). The easternmost floats are entrained in the NEUC and after about five years, they either return close to their original location through the tropical recirculation, or exit the isopycnal in the Guinea Dome upwelling region. It is striking to note how close these integrated trajectories are to the Bernoulli isolines of the annual mean circulation. To avoid an overloaded figure, we invite the reader to superimpose Figure 7 and Figure 13 to check the high degree of similarity between the trajectories and the B field.

[33] In the south (Figure 14), the September outcrop line is very close to the equator (Figure 12b); hence this isopycnal does not illustrate best the connections between subtropics and tropics. However, it is characteristic of the ventilation of the tropical thermocline at low latitudes. The same patterns as observed in the annual mean circulation mark the trajectories: a wide window of equatorward pathways passing through the western boundary and the interior, as well as recirculation within the Angola gyre and eventual exit into the mixed layer. In the western half of the basin floats take less than 2 years to reach the equator, whereas in the east it takes 3 to 4 years to circulate out of the Angola gyre. Again there is a striking similarity between the trajectories and the annual mean flow described by the Bernoulli function in Figure 7.

[34] These results suggest that the seasonal tropical circulation results in isopycnal flow pathways comparable to those inferred from the annual mean flow in terms of the location of the particles throughout their journey. The synthetic float diagnostic at shallower and deeper isopycnals of the thermocline comes to the same conclusion (not shown). In addition we computed trajectories starting in the late summer of both hemispheres. The ventilation of the thermocline can result from the propagation of anomalous signals (negative temperature anomaly; in particular, see *Lazar et al.* [2001]) that could have subducted during

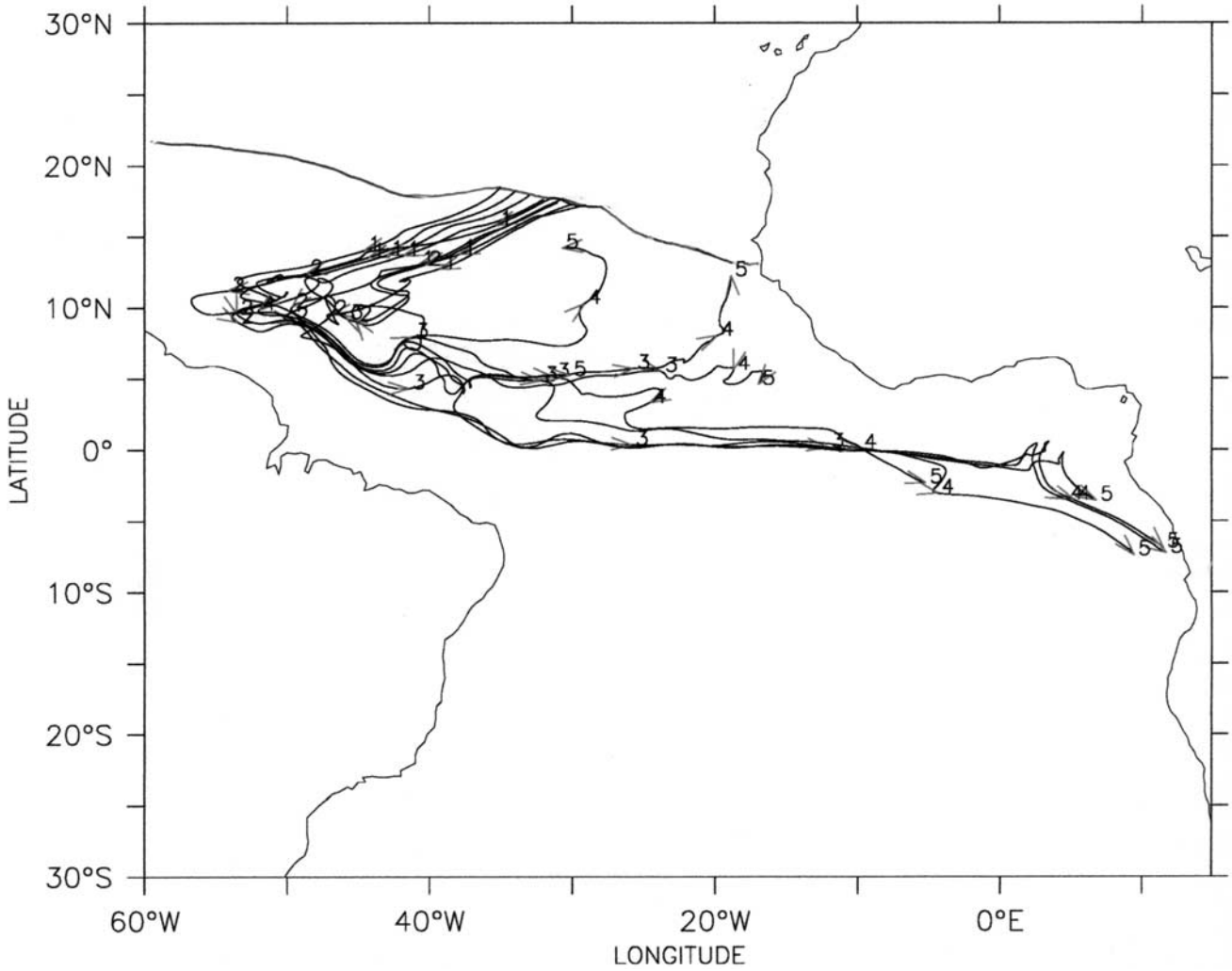

Figure 13. Trajectories of floats over five years, released in the seasonal circulation along the isopycnal $\sigma = 25$ shown on Figure 7; the release was at the northern outcrop line in March and over the narrow window feeding the tropical thermocline. For one particle trajectory, each number and associated arrowhead corresponds to the duration in year and the position at the end of each year.

summer. However, the result is the same; trajectories still follow rather closely the annual mean Bernoulli contours.

[35] In the Southern Hemisphere, this result is not surprising since the seasonal variability of the circulation pathways is very small within the subsurface SEC. In the north, one could expect more discrepancies between the two set of trajectories. To compare in a more definite and general manner the time-integrated advection by annually averaged versus seasonal velocity fields, a detailed study of the sensitivity of mean float trajectories to the seasonal cycle should be carried out in this region. A very large number of particles should be analyzed, especially with a focus on the impact of different resolution in time (role of short-term circulation events) and space (role of eddy mixing). Hence, our comparison must be considered as specific to our set of simulations, since other models or different model configurations could produce more differences between trajectories. Finally, it is worth noting that a companion paper [*Inui et al.*, 2002] with the same model shows that annual mean surface forcing creates a circulation very close to the annual average of the seasonally forced circulation. Consequently the long-term float trajectories and pathways are very similar in the two papers.

[36] To check if the timescales of these trajectories are also in agreement with the steady circulation, we released floats on the annual mean isopycnal $\sigma = 25$ and computed their trajectories using annual mean currents (Figure 15). Here the initial locations of the floats are along the annual mean outcrop line of the isopycnal and are consequently different from the seasonal outcrop line, especially in the south where the seasonal migration is larger. Considering this difference, it appears that for comparable initial positions, the timescales are often larger, up to one year, than those of the seasonal circulation. This difference is due to the smoothing effect of the annual average over the velocities.

[37] In order to compare with available observations, we also derived float trajectories based on climatological hydrography, the annual mean Levitus and Boyer data.

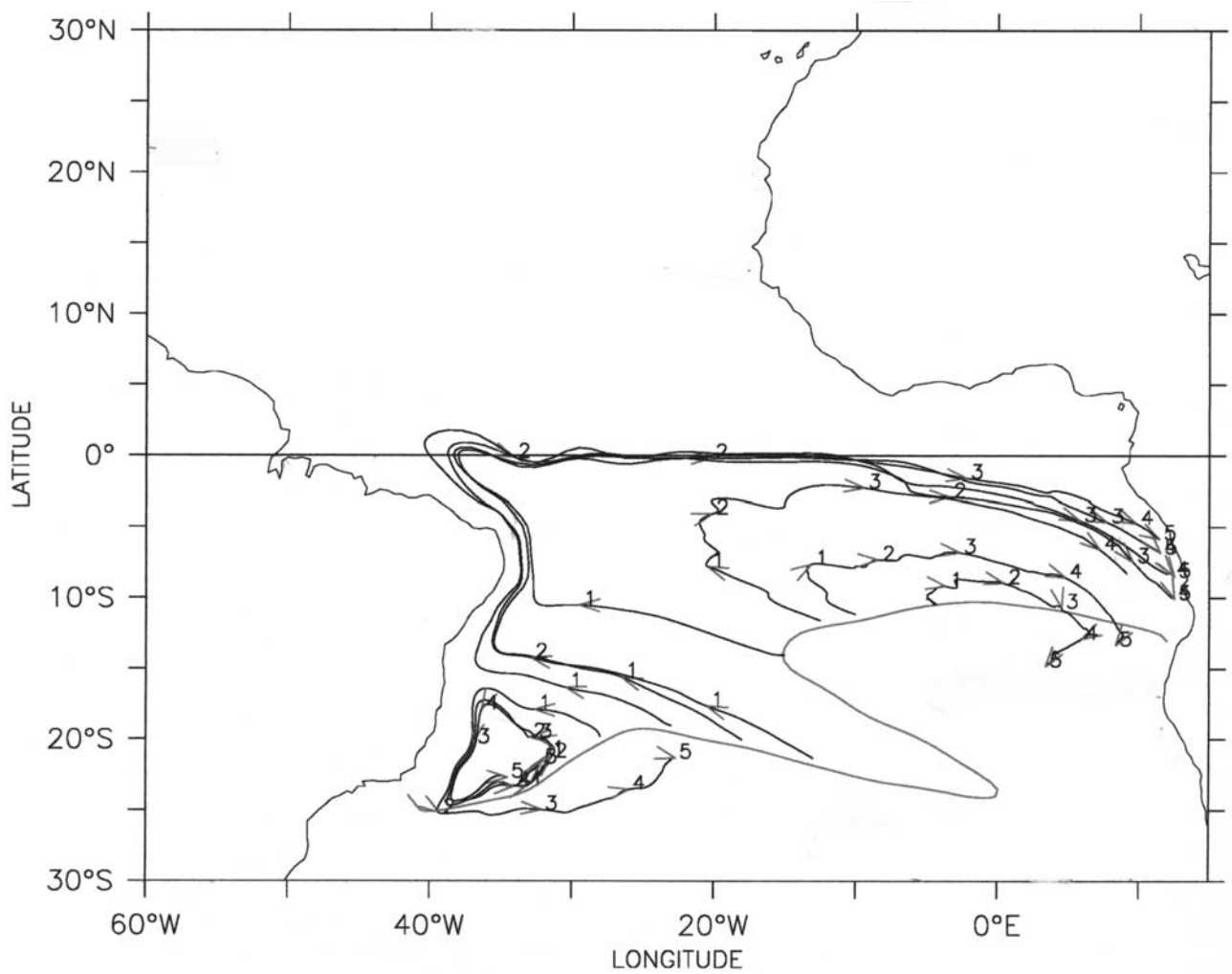

Figure 14. Same as in Figure 13 but for releases at the southern outcrop line in September.

The horizontal velocity vector used to calculate the Lagrangian trajectories was computed as

$$\mathbf{V}(\sigma) = -\frac{1}{\rho_0 f}\mathbf{k} \times \nabla B(\sigma).$$

with **k** the vertical unity vector, and B the Bernoulli function shown Figure 11a. As shown in Figure 16, the timescale and the pathways of the trajectories are similar to those of the model in the north with a transit time of five to six years from the outcrop until the equatorial region or the boundaries are reached. In the south, the trajectories within the SEC are similar to the model trajectories but, as noted earlier for the Bernoulli function, the lack of the Angola gyre in the circulation means that no particles follow its recirculation.

[38] There is no doubt that the density gradients of the Levitus and Boyer data set, like our annual average, are far smoother than the synoptic field, and this leads to slow particle displacements. For the ventilation of the equatorial thermocline, it is mainly the open ocean subsurface velocities within the sSEC that set the lower limit of the water mass trajectory timescales. The most recent estimate from observations that we found of these velocities was a geostrophic computation by *Stramma* [1991] based on a March synoptic section at 15°W going from 5°S to 15°S. The southern branch of the SEC had a maximum at 13°S where the flow decreased from 10^{-1} ms^{-1} at the surface to 5×10^{-2} m s^{-1} at 200 m depth. This velocity range corresponds well to our March field (Figure 12a) that reaches the same subsurface value. This favorable comparison enhances our confidence in the timescales of the STC provided by our computations. Therefore we conclude that the simulated annual mean circulation of the tropical Atlantic thermocline contains enough information to determine the geographical characteristics of the several-year journeys of the water masses after subduction. Figure 15 constitutes a good summary representation of the subsurface circulation within this model domain in terms of pathways. Its timescales, ranging from 3 to 6 years, are slightly overestimated (by less than a year) compared to trajectories within the seasonal circulation.

5. Discussion and Conclusion

[39] The tropics correspond to the regions of the ocean that connect the equator and the subtropical ocean subbasins. It has been suggested that heat exchange across

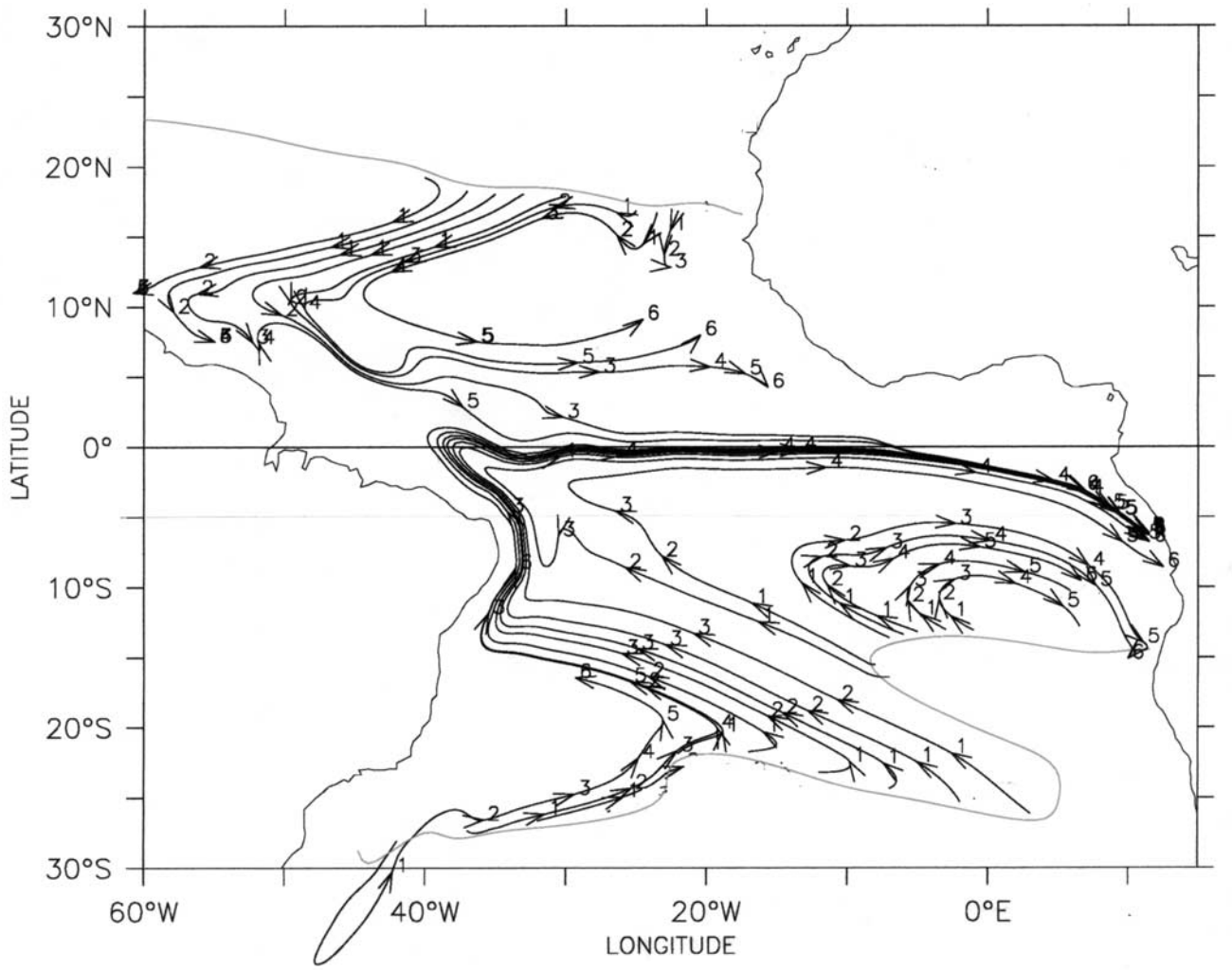

Figure 15. Same as Figure 13 but the floats are advected by the circulation in annual mean along the isopycnal $\sigma = 25$.

these latitudes could constitute oceanic components of interannual to decadal coupled modes of low-latitude climate variability. Circulation at these latitudes is schematically organized in shallow subtropical-tropical cells (STC) having multiyear timescales for the subsurface flow paths. Interannual to decadal variability strongly modulates the climate of the tropical Atlantic, and it is therefore a region where these connections ought to be investigated. The knowledge of the thermocline branches of the STCs is far from being enough for a quantification and understanding of their role in these low-frequency modulations. Also, the processes of thermocline water formation and destruction have received much less attention in the tropics than at subtropical and mid latitudes, and this paper provides new information on when and how the low-latitude and equatorial thermocline is ventilated.

[40] Like in the Pacific, the obduction (often called upwelling) regions in the tropical Atlantic are localized in the eastern basin, however their spatial extent is far larger, reaching at least one third of the tropical zone. Consequently, thermocline water entrainment (or upwelling) will play a role in the control of the mean SST and its variability over a greater portion of the basin as compared to the Pacific. If this role is proven significant compared to surface processes at certain frequencies (it has not been shown yet), the STC, which feed these obduction regions, are likely to have an impact on the variability of tropical ocean-atmosphere coupled features like the Intertropical Convergence Zone, or the African monsoon.

[41] It is striking to see how different the tropical subduction and obduction rates are when the weaker winds from the *Da Silva et al.* [1994] climatology are used. The rates decrease by a factor close to two due to weaker absolute value of Ekman currents as well as weaker divergence and convergence. First, this illustrates the sensitivity of water renewal rates in the subtropical-tropical cells to wind intensity. Second, it underlines the requirement to reduce uncertainties in the wind forcing over the ocean to accurately quantify the impact of the subtropical-tropical oceanic subsurface connections on the variability of the tropical Atlantic SST.

[42] Consistent with previous studies, the annual subduction rates presented here were computed as advective fluxes using a purely kinematic calculation. The contribution of

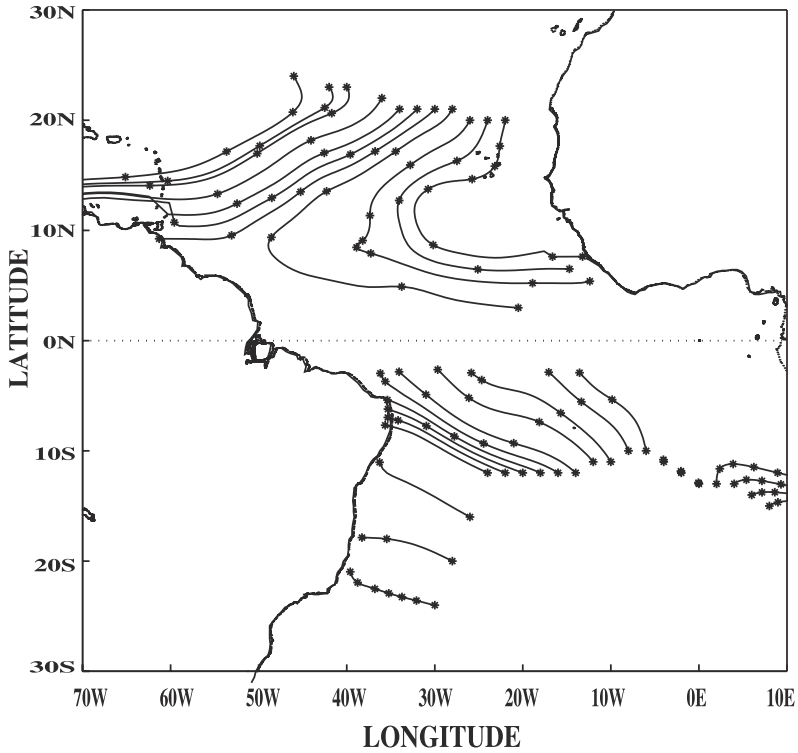

Figure 16. Trajectories of floats advected by the geostrophic circulation computed from *Levitus and Boyer* [1994] data in annual mean along the isopycnal $\sigma = 25.5$; each asterisk corresponds to the position of the particle every year.

mixing to the annual subduction of thermocline waters was neglected. However, *Marshall et al.* [1999] showed that within the tropics of their North Atlantic model, in zonal average, the advective fluxes are not able to carry away all the buoyancy supplied by air-sea fluxes, and that some vertical mixing must complete the transfer. They suggested, following *McWilliams et al.* [1996], that this mixing might occur principally in the upwelling regions off the coast of Africa. In agreement with these results, *Nurser et al.* [1999] showed in an isopycnal OGCM of the North Atlantic that vertical mixing in tropical upwelling regions and eastern boundary is essential in consuming the intermediate water of the thermocline. However, these latter authors found that the corresponding density transfer (lightening) achieved by mixing is still driven by advection through the bottom of the mixed layer. These results imply that our rate estimates must be taken with caution in the tropical upwelling regions. Further sensitivity studies should quantify in detail the horizontal distribution of vertical mixing and the associated surface sinks of tropical thermocline water.

[43] Regarding the timing of the subduction, we addressed the matter by quantifying the duration of subduction, and the month when subduction starts. Knowledge of both is needed to understand and quantify how the properties of the thermocline water are set at the surface. Whereas previous observations and modeling studies that focused on higher latitudes indicated that subduction starts at the end of winter, our analysis reveals a large span of starting time in the low subtropics and tropics, ranging from mid winter to late spring in the two hemispheres, with earlier times in the low subtropics and later times closer to the equator. A gross comparison with observations tends to confirm our results. Time of subduction initiation is explained by the seasonal cycle of the trade and westerly winds, in which speed decreases allow for mixed layer restratification by the short wave flux. This result shows that wind forcing is controlling water mass formation not only through its curl (driving subduction rates) and control of latent heat flux (determining temperature and salinity characteristics), but also through control of the subduction season (having an additional effect on water mass characteristics). It emphasizes how the sustenance and variability of the equatorial thermocline depend on the variability of the wind forcing in the Southern Hemisphere (main source of the equatorial undercurrent), and underlines again the necessity to reduce uncertainties in the wind forcing over this region. Our experiments that partitioned the control of subduction between wind and radiative forcing also provide insight into what regions may be susceptible to climate variability and change in wind and shortwave radiation forcing.

[44] The second part of our study was aimed at providing a synthetic picture of the circulation and long-term evolution of the subducted tropical water masses. The large seasonal variations in circulation were emphasized in the Northern Hemisphere in relation to the seasonal migration of the ITCZ. In the south, it appears that the flow pathways are less variable. Rather, it is the isopycnal outcrop position that varies strongly. Considering these significant variations, we followed particles along isopycnals over five-year periods, the approximate maximum time necessary for water particles to travel from an outcrop line to the equator or

back to the outcrop or tropical obduction region. In the context of low-frequency variability studies associated with potential coupled ocean-atmosphere modes, this five-year timescale is the longest timescale associated with simple advection of (salinity compensated) heat anomalies within the subsurface branches of the Atlantic STC. It corresponds well to results of simulations carried out with the same model and studying the subduction and subsurface displacement of artificially imposed SST anomalies within the SEC [*Lazar et al.*, 2001].

[45] Obviously, the trajectories within a climatological circulation do not take into account the low-frequency variability of the pathways. The significance of the interannual to decadal variability of the subsurface circulation needs to be quantified especially in terms of its impact on the multiyear trajectories. Current extensions of this work are aimed at quantifying the impact of interannual to decadal variations of the atmosphere forcing on the subsurface branches of the subtropical-tropical cells and the integrated trajectories.

[46] **Acknowledgments.** We thank Sabine Arnault, J. Toole, and two anonymous reviewers for constructive comments.

References

Blanke, B., M. Arhan, G. Madec, and S. Roche, Warm water paths in the equatorial Atlantic as diagnosed with a general circulation model, *J. Phys. Oceanogr.*, *29*, 2753–2768, 1999.

Blanke, B., M. Arhan, G. Prévost, and A. Lazar, A Lagrangian numerical investigation of the origins and fates of the salinity maximum water in the Atlantic, *J. Geophys. Res.*, *107*, 10.1029/2002JC001318, in press, 2002.

Chen, D., L. M. Rothstein, and A. J. Busalacchi, A hybrid vertical mixing scheme and its application to tropical ocean models, *J. Phys. Oceanogr.*, *24*, 2156–2179, 1994.

Cushman-Roisin, B., *Dynamics of the Oceanic Surface Mixed Layer*, edited by P. Muller and D. Henderson, pp. 181–196, Hawaii Inst. of Geophys., Honolulu, Hawaii, 1987.

Da Silva, A., A. C. Young, and S. Levitus, *Atlas of Surface Marine Data 1994*, vol. 1, *Algorithms and Procedures, NOAA Atlas NESDIS 6*, U.S. Dep. of Commer., Washington, DC, 1994.

De Miranda, A. P., B. Barnier, and W. K. Dewar, Mode waters and subduction rates in a high-resolution South Atlantic simulation, *J. Mar. Res.*, *57*, 213–244, 1999.

Gent, P. R., and M. A. Cane, A reduced gravity, primitive equation model of the upper equatorial ocean, *J. Comput. Phys.*, *81*, 444–480, 1989.

Gu, D. F., and S. G. H. Philander, Interdecadal climate fluctuations that depend on exchanges between the tropics and extratropics, *Science*, *275*, 805–807, 1997.

Hastenrath, S., and J. Merle, The annual march of heat storage and export in the tropical Atlantic Ocean, *J. Phys. Oceanogr.*, *16*, 694–708, 1986.

Hellerman, S., and M. Rosenstein, Normal monthly wind stress over the world ocean with error estimates, *J. Phys. Oceanogr.*, *13*, 1093–1104, 1983.

Huang, R. X., and J. Pedlosky, Climate variability inferred from a layered model of the ventilated thermocline, *J. Phys. Oceanogr.*, *29*, 779–790, 1999.

Inui, T., A. Lazar, P. Rizzoli, and A. J. Busalacchi, Wind stress effect on the subtropical-tropical circulation in the Atlantic, *J. Phys. Oceanogr.*, in press, 2002.

Kraus, E. B., and J. S. Turner, A one-dimensional model of the seasonal thermocline, II, The general theory and its consequences, *Tellus*, *19*, 98–105, 1967.

Kröger, J., Mechanismen meridionaler transportprozesse im tropischen Atlantik, Ph.D. thesis, 153 pp., Christian-Albrechts Univ. zu Kiel, Kiel, Germany, 2001.

Lazar, A., R. Murtugudde, and A. J. Busalacchi, A model study of temperature anomaly propagation from the subtropics to the tropics within the south Atlantic thermocline, *Geophys. Res. Lett.*, *28*, 1271–1274, 2001.

Lee, S. K., and G. T. Csanady, Warm water formation and escape in the upper tropical Atlantic Ocean, 2, A numerical model study, *J. Geophys. Res.*, *104*, 29,573–29,590, 1999.

Levitus, S., T. Boyer, *World Ocean Atlas*, vol. 4, *Temperature. NOAA Atlas NESDIS 4*, U.S. Dep. of Commer., Washington, D.C., 1994.

Lu, P., and J. P. McCreary, Influence of the ITCZ on the flow of thermocline water from the subtropical to the equatorial Pacific Ocean, *J. Phys. Oceanogr.*, *25*, 3076–3088, 1995.

Malanotte-Rizzoli, P., K. Hedstrom, H. Arango, and D. B. Haidvogel, Water mass pathways between the subtropical and tropical ocean in a climatological simulation of the North Atlantic Ocean circulation, *Dyn. Atmos. Oceans*, *32*, 331–371, 2000.

Marshall, D., and J. C. Marshall, On the thermodynamics of subduction, *J. Phys. Oceanogr.*, *25*, 138–151, 1995.

Marshall, J. C., A. J. G. Nurser, and R. G. Williams, Inferring the subduction rate and period over the North Atlantic, *J. Phys. Oceanogr.*, *23*, 1315–1329, 1993.

Marshall, J. C., D. Jamous, and J. Nilsson, Reconciling thermodynamic and dynamic methods of computation of water-mass transformation rates, *Deep Sea Res.*, *46*, 545–572, 1999.

McWilliams, J. C., G. Danabasoglu, and P. R. Gent, Tracer budgets in the warm water sphere, *Tellus, Ser. A*, *48*, 179–192, 1996.

Murtugudde, R., and A. J. Busalacchi, Salinity effects in a tropical ocean model, *J. Geophys. Res.*, *103*, 3283–3300, 1998.

Murtugudde, R., J. McCreary, and A. J. Busalacchi, Oceanic processes associated with anomalous events in the Indian Ocean with relevance to 1997–1998, *J. Geophys. Res.*, *105*, 3295–3306, 2000.

Nurser, A. J. G., R. Marsh, and R. G. Williams, Diagnosing water mass formation from air-sea fluxes and surface mixing, *J. Phys. Oceanogr.*, *29*, 1468–1487, 1999.

Oberhuber, J., An atlas based on "COADS" data set, *Rep. 15*, Max Planck Inst. für Meteorol., Hamburg, Germany, 1988.

Qiu, B., and R. X. Huang, Ventilation of the North Atlantic and North Pacific: Subduction versus obduction, *J. Phys. Oceanogr.*, *25*, 2374–2390, 1995.

Rothstein, L. M., R. H. Zhang, A. J. Busalacchi, and D. Chen, A numerical simulation of the mean water pathways in the subtropical and tropical Pacific Ocean, *J. Phys. Oceanogr.*, *28*, 322–343, 1998.

Schneider, N., A decadal spiciness mode in the tropics, *Geophys. Res. Lett.*, *27*, 257–260, 2000.

Schneider, N., A. J. Miller, M. A. Alexander, and C. Deser, Subduction of decadal Pacific temperature anomalies: Observations and dynamics, *J. Phys. Oceanogr.*, *29*, 1056–1070, 1998.

Seager, R., B. Blumenthal, and Y. Kushnir, An advective atmospheric mixed layer model for Ocean modeling purpose: Global simulation of surface heat fluxes, *J. Clim.*, *8*, 1951–1964, 1995.

Servain, J., Simple climatic indexes for the tropical Atlantic-ocean and some applications, *J. Geophys. Res.*, *96*, 15,137–15,146, 1991.

Stramma, L., Geostrophic transport of the south equatorial current in the Atlantic, *J. Mar. Res.*, *49*, 281–294, 1991.

Stramma, L., and M. England, On the water masses and mean circulation of the South Atlantic Ocean, *J. Geophys. Res.*, *104*, 20,863–20,883, 1999.

Stramma, L., and F. Schott, The mean flow field of the tropical Atlantic Ocean, *Deep Sea Res.*, *46*, 279–303, 1999.

Williams, R. G., M. A. Spall, and J. C. Marshall, Does Stommel's mixed layer "demon" work?, *J. Phys. Oceanogr.*, *25*, 3089–3102, 1995.

Wilson, W. D., E. Johns, and R. L. Molinari, Upper layer circulation in the western tropical North Atlantic ocean during August 1989, *J. Geophys. Res.*, *99*, 22,513–22,523, 1994.

A. J. Busalacchi, A. Lazar, and R. Murtugudde, ESSIC, University of Maryland, College Park, MD 20742-2425, USA. (ala@lodyc.jussieu.fr; tonyb@essic.umd.edu; ragu@vinsanto.essic.umd.edu)

T. Inui, International Arctic Research Center, University of Alaska, Fairbanks, 30 Koyokuk Drive, Fairbanks, AK 99775, USA. (tomoko@iarc.uaf.edu)

P. Malanotte-Rizzoli, MIT, 77 Massachusetts Avenue, Cambridge, MA 02139-4307, USA. (rizzoli@mit.edu)

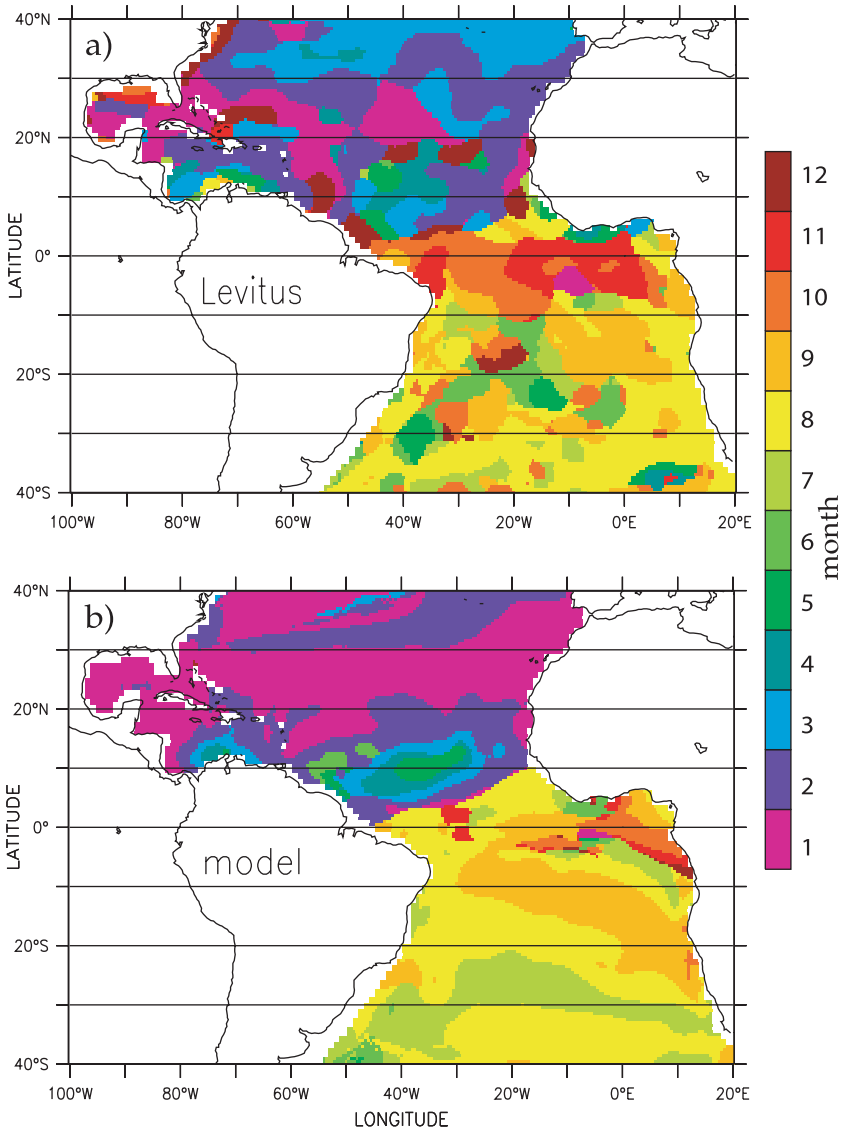

Figure 2. Horizontal distribution of the month (from 1 to 12 for January to December) of deepest mixed layer. (a) *Levitus and Boyer* [1994] data set. (b) Reference simulation.